Evaluation Methods of Vertical Subgrade Reaction Modulus and Rotational Resistance Moment for Seismic Design of Embedded Foundations

Takashi Nagao
Research Center for Urban Safety and Security
Kobe University
Kobe City, Japan
nagao@people.kobe-u.ac.jp

Ryota Tsutaba
Ex-Faculty of Engineering
Kobe University
Kobe City, Japan
ryota.ttb.0511@gmail.com

Abstract-In a seismic design of embedded foundations, the vertical Subgrade Reaction (SR) acting on a foundation bottom surface and the Rotational Resistance Moment (RRM) generated by the SR are calculated using an SR Modulus (SRM). The SRM and RRM depend on both ground rigidity and Foundation Width (FW). However, the SRM and RRM calculation methods adopted in design codes might not properly consider their FW dependency. In this study, SRM and RRM evaluation methods for embedded foundations subjected to a seismic load were examined by conducting a two-dimensional finite element analysis under the condition where ground rigidity and FW were changed considering the nonlinearity of the ground. The results show that when the seismic load is large and the nonlinearity of the ground appears, the SR distribution is different from the assumption in the design code. The FW dependency of the SRM was lower than the assumption of the design code. Furthermore, methods to calculate the SRM and RRM in accordance with the FW and ground rigidity are proposed.

Keywords-subgrade reaction modulus; rotational resistance moment; foundation width

I. INTRODUCTION

A structure's foundation must ensure stability by transmitting the applied load to the ground. When the structure is heavy or the ground is soft, a columnar foundation is embedded in a sufficiently strong soil layer. In addition to a vertical load, such as the deadweight of the structure, a seismic load acts horizontally during an earthquake, rotating the structure. The vertical Subgrade Reaction (SR) acting on the foundation bottom supports the vertical load and generates a Rotational Resistance Moment (RRM) to contribute to the structure's rotational resistance. The SR is calculated by multiplying the foundation's displacement and a SR Modulus (SRM). The SRM depends on the ground rigidity and Foundation Width (FW) and increases with the increase in ground rigidity and decreases with the increase in FW [1-3]. Therefore, various design codes, such as the Japanese Specifications for Highway Bridges (JSHB) [4], apply the SRM calculation equation in accordance with the FW. When the seismic load is large or when a large lateral spreading pressure is considered to act during an earthquake [5], the FW should be widened to enhance seismic resistance. However, when using the SRM calculation equation adopted in the design code, the SRM significantly decreases as the FW increases, and an increase in the SR proportional to the increase in the FW cannot be expected. Therefore, the FW should be extremely wide when the seismic load is large. However, the results of the horizontal loading test of pier models where the FW was changed revealed that the seismic resistance becomes extremely high by widening the FW because the vertical SR becomes large [6]. It has been also highlighted that the FW dependence of the vertical SRM is lower than that of the horizontal SRM [7]. Therefore, the horizontal and vertical SRMs should be evaluated differently, and the appropriate evaluation of the vertical SRM is critical to perform rational seismic design. In this study, a two-dimensional finite element analysis was conducted considering the nonlinearity of the ground. From the analysis results, evaluation methods for the vertical SRM and RRM for embedded foundations subjected to seismic loads are proposed. Since only vertical SR and SRM are considered in this paper, they are described as SR and SRM for simplicity in the following.

II. METHOD

A. Analytical Model

Two-dimensional finite element analysis was used to evaluate the characteristics of the SR to embedded foundations under seismic loading. The analysis code used is FLIP [8], which is widely used for the evaluation of the seismic stability of structures [9]. A foundation of 20m height was assumed to be 10m embedded, and the ground was modeled to a depth of 30m. To evaluate the difference in the SRM because of the difference in the FW, four cases with FWs (B) of 4, 6, 8, and 10m were set. Figure 1 shows an analytical model and a finite element mesh diagram, taking the case of B = 4m as an example. The mesh height and width for structural and surrounding ground elements were set at 0.5m, which are smaller than those for other elements. The foundation was modeled using linear planar elements, assuming a reinforced concrete structure, with Young's modulus of $E = 2.5\times10^7$kN/m^2, Poisson's ratio of $\nu = 0.20$, and density of

Corresponding author: Takashi Nagao

ρ = 2.4t/m^3. For the ground, density ρ = 1.8t/m^3 and Poisson's ratio ν = 0.33 were used. Three cases of soft ground (Case A), intermediate ground (Case B), and hard ground (Case C) were set using the *N*-values obtained from the standard penetration test (Table I).

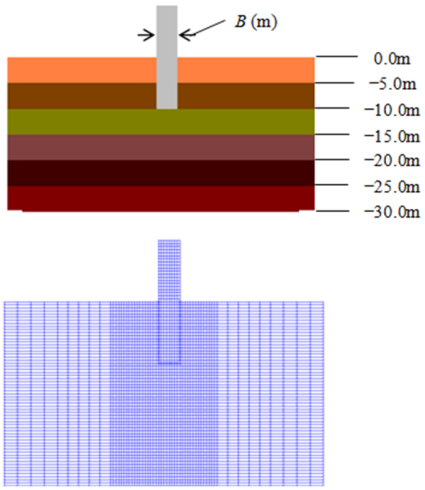

Fig. 1. Analysis model and finite element mesh diagram.

TABLE I. GROUND CONDITIONS (*N*-VALUES)

Depth(m)	Case A	Case B	Case C
0.0 to -5.0	10	10	10
-5.0 to -10.0	10	10	30
-10.0 to -30.0	10	30	50

The ground shear rigidity in the middle of each stratum is called the reference shear rigidity and is calculated by [10]:

$$G_{ma} = 14100\, N_{131}{}^{0.68} \quad (1)$$

where G_{ma} is the reference shear rigidity (kN/m^2) and N_{131} is the equivalent *N*-value for the reference effective overburden pressure of 131kN/m^2. The ground shear rigidity G_m at each depth is calculated using [11]:

$$G_m = G_{ma}\left(\frac{\sigma_m{}'}{\sigma_{ma}{}'}\right)^{0.5} \quad (2)$$

where G_m is the shear rigidity, G_{ma} is the reference shear rigidity, σ_m' is the effective confining pressure, and σ_{ma}' is the reference effective confining pressure corresponding to the reference shear rigidity.

Young's modulus of the ground is calculated using:

$$E_m = 2(1+\nu)G_m \quad (3)$$

where E_m is Young's modulus, G_m is the shear rigidity and ν is the Poisson's ratio.

The ground shows remarkable nonlinearity when the shear strain exceeds 10^{-6}. In this study, the nonlinearity of the ground is expressed as in (4) using a hyperbolic model [12]:

$$\frac{G}{G_0} = \frac{1}{1+\frac{G_0\gamma}{\tau_m}} \quad (4)$$

where G is the shear rigidity, G_0 is the initial shear rigidity, γ is the shear strain, and τ_m is the shear strength, which is calculated using [10]:

$$\tau_m = \sigma_m' \sin\phi \quad (5)$$

where σ_m' is the effective confining pressure and ϕ is the shear resistance angle.

By calculating the relative density using (6), the shear resistance angle is calculated using (7) [10]. The ground shear resistance angles under the foundation bottoms of Cases A, B, and C are 39.0°, 40.7°, and 42.5°, respectively.

$$Dr = 21\left(\frac{100\,N_{131}}{\sigma_v{}'+70}\right)^{0.5} \quad (6)$$

$$\varphi = 0.0003Dr^2 + 0.0426Dr + 36.682 \quad (7)$$

where Dr is the relative density (%) and σ_v' is the reference effective overburden pressure (131kN/m^2).

Slipping or separation can occur on the contact surface between the foundation and the ground. To express these phenomena, joint elements are installed between the structure and the ground. The joint element transmits a compressive force corresponding to the initial rigidity perpendicularly to the element, whereas the tensile force is not transmitted, reproducing the separation of the ground and the structure. For the sliding direction, shear force corresponding to the initial shear rigidity is transmitted until the shear stress reaches shear strength.

B. Analysis Method

The analysis was conducted in two stages. At first, the deadweight of the foundation was applied, and afterwards the horizontal load was applied. The loading position of the horizontal load was set to be the top of the foundation to increase the rotational moment. Table II shows the loads applied for each FW.

TABLE II. LOADS

FW (m)	Horizontal load (kN)	Dead weight (kN)
4	1000	1920
6	1500	2880
8	1500	3840
10	1800	4800

To stabilize the analysis, the load was made zero for the first second and was gradually increased. Calculations were performed with 1000Hz sampling for deadweight loading and 400Hz for horizontal loading. The loading rates were 2000kN/s and 200kN/s for the deadweight and horizontal loading respectively and the calculation was continued for 1s after the maximum load was reached. Figure 2 shows the time history of the horizontal load. The SRM is calculated using:

$$k_v = \frac{\sigma}{dy} \quad (8)$$

where k_v is the SRM (kPa/m), σ is the normal stress (kPa) of the joint element, and dy is the vertical displacement of the foundation (m).

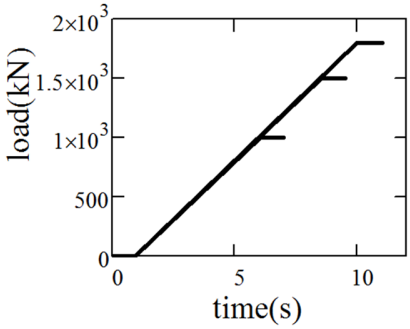

Fig. 2. Time history of horizontal loading.

III. RESULTS AND DISCUSSION

A. Comparison of SR in this Study and in JSHB

Figure 3 shows the time history of the SR and foundation displacement during horizontal loading, referring to B = 4m and 10m for Case B respectively. The values in the legend indicate distances from the foundation edge on the side where settlement occurs. Downward displacement is defined as negative.

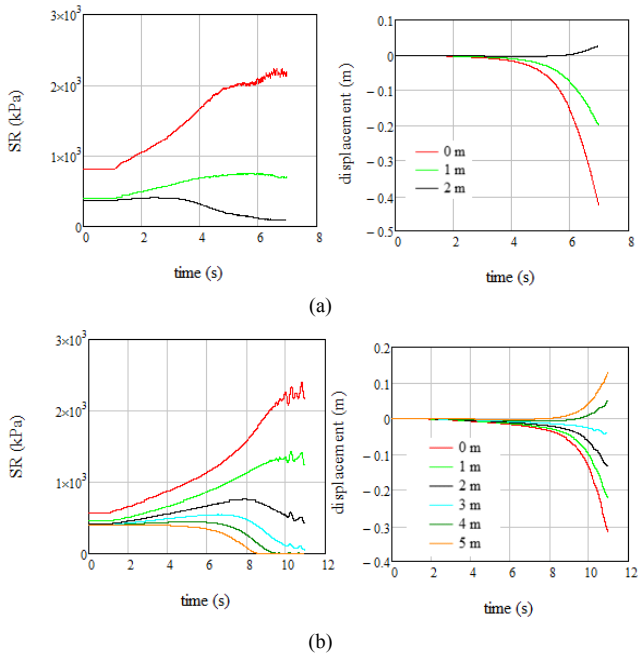

Fig. 3. Time history of SR and displacement. (a) B = 4m , (b) B = 10m.

The SR shows a larger value as it moves closer to the foundation edge. Especially at the foundation edge, the initial SR value is larger than those at other positions, correlating with the results of [7]. Focusing on the SRs at 1m, after 5s, when B = 4m, and after 9s, when B = 10m, they show almost constant values. However, the SR at the foundation edge continues to increase for 9–10s, where the horizontal load continues to increase, especially for B = 10m. The displacement continues to increase after the SR reaches the maximum value at each position, indicating that the ground shows strong nonlinearity and yielding occurs. Furthermore, at 2m from the foundation edge with B = 4m, the SR decreases after 4s, and the foundation displaces upward. Foundation rotation occurs at a position shorter than half of the FW. The result for B = 10m is similar. The SR decreases after 8s at 3m from the foundation edge, and upward displacement occurs at 4m from the foundation edge. This result is compared with the assumption of the JSHB [4]. The JSHB assumes that the rotational center is at the foundation's center, and the SR is increased to the allowable bearing capacity with increasing horizontal load, regardless of the position. Figures 4(a)-(b) show the assumption of the JSHB. Figure 4(a) shows the SR distribution when the SR at the foundation edge has reached the allowable bearing capacity (q_a). As the horizontal load increases, the SR in the range up to the center of the foundation increases until it reaches the allowable bearing capacity (Figure 4(b)). The allowable bearing capacity is calculated using:

$$\begin{aligned} q_d &= \frac{1}{2}\beta\gamma_1 B N_r + \gamma_2 D_f N_q \\ q_a &= \frac{1}{F_S}\left(q_d - \gamma_2 D_f\right) + \gamma_2 D_f \\ N_q &= \frac{1+\sin\varphi}{1-\sin\varphi} exp\left(\pi \tan\varphi\right) \\ N_r &= \left(N_q - 1\right)\tan\left(1.4\varphi\right) \end{aligned} \quad (9)$$

where q_d is the ultimate bearing capacity of the ground, β is the shape factor of the foundation bottom, e.g. 0.8 for square, γ_1 and γ_2 are the unit weights of the ground below and above the foundation bottom respectively, B is the FW, D_f is the foundation embedded depth, q_a is the allowable bearing capacity of the ground, Fs is the safety factor (2 in the event of an earthquake), and ϕ is the shear resistance angle of the ground. Figure 4(c) shows the SR distribution of this study. Maximum SR is smaller than the allowable bearing capacity of the JSHB and the rotational center is not necessarily at the foundation's center.

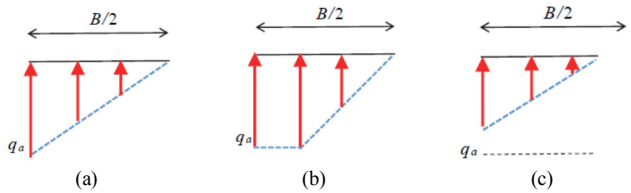

Fig. 4. SR distribution.

Figure 5 compares the allowable bearing capacity from the JSHB and the maximum SR at the foundation edge obtained in this study. The horizontal axis is the shear resistance angle of

the ground at the foundation bottom. The maximum SRs obtained in this study are smaller than the allowable bearing capacities of the JSHB. The JSHB sets the allowable bearing capacity lower than the ultimate bearing capacity by introducing the safety factor, however, it still overestimates the maximum SR. Furthermore, in the JSHB, the allowable bearing capacity increases as the FW increases, but in this analytical result, the change in the maximum SR with the change in the FW is slight. The allowable bearing capacity calculation equation adopted in the JSHB is conventional for the condition that only a vertical load is applied and is not applicable when an inclined load is applied. In addition to overestimating the SR distribution, the JSHB overestimates the RRMs by assuming that the rotational center is always at the foundation's center.

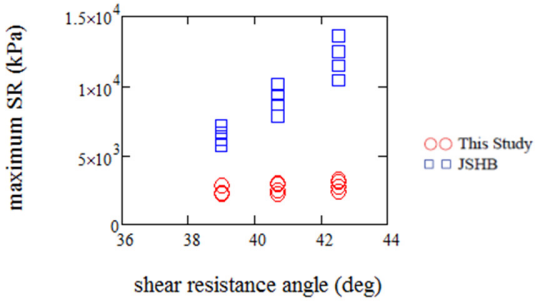

Fig. 5. Comparison of maximum SR.

B. Ground Stress Characteristics under Inclined Loading

When the foundation is subjected to an inclined loading, both compressive and shear strains are generated in the ground under the foundation. Figure 6 shows the time histories of the compressive strain and shear strain in the ground under the foundation for the condition B = 4m of Case A. The legend is the distance from the foundation edge. The compressive strain value is the largest at the foundation edge and decreases toward the foundation's center. In contrast, no noticeable difference occurs in the shear strain because of the difference in the position from the foundation edge.

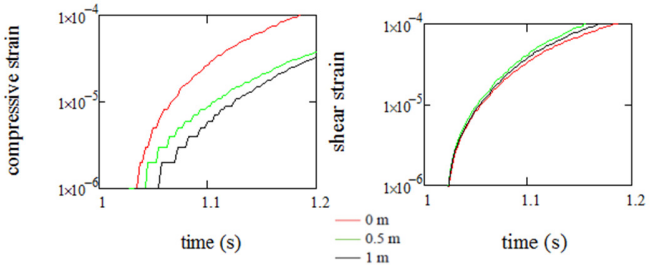

Fig. 6. Ground stress characteristics.

The compressive strain differs from location to location because it depends on the amount of foundation settlement. However, the shear strain depends on the foundation's rotational angle because the foundation is rigid and bending deformation does not occur. Therefore, no significant difference occurs in the shear strain according to the distance from the foundation edge. The relationship between shear stress and shear strain is nonlinear with increasing strain, and when the shear stress reaches a value close to the shear strength, the shear strain increases abruptly without an increase in the shear stress. Therefore, the nonlinear behavior appears simultaneously regardless of the distance from the foundation edge. Thus, the SR at positions other than the foundation edge does not reach the maximum value at the foundation edge, and the relationship between the SR and settlement shows nonlinearity.

C. Evaluation Method of SRM

Figure 7 shows the time histories of the SRM, referring to the conditions B = 4m and 10m of Case B. The legend is the distance from the foundation edge. At the foundation edge, the SR is large because of the influence of boundary conditions and the SRM is larger than those at other positions, correlating with the result in [7]. In the early stage of loading, the SRM shows a constant value because the ground does not exhibit nonlinear behavior. The SRM decreases because of the effect of the nonlinear properties of the ground after 4s at B = 4m, and after 6s at B = 10m. We excluded the data at the foundation edge and obtained the average SRM value for the range in which it shows a constant value. From the results, the calculation equation (10) of the SRM was obtained. The SRM calculation equation in the JSHB is shown in (11). The SRM calculation equation in this study has a weaker FW dependency than that in the JSHB, correlating with [7].

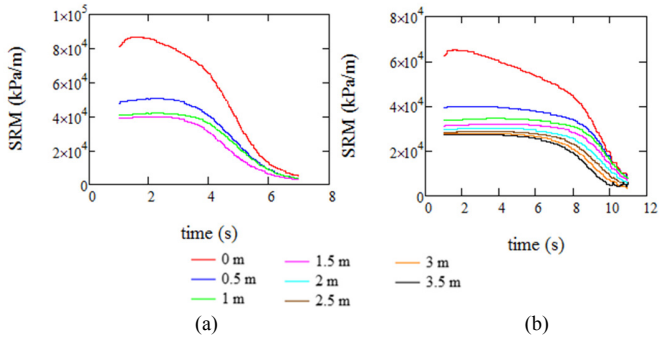

Fig. 7. Time history of SRM. (a) B = 4m, (b) B = 10m

$$k_v = 0.15\frac{E_m}{B_r}\left(\frac{B}{B_r}\right)^{-\frac{1}{2}} \quad (10)$$

$$k_v = \frac{1}{0.3}\alpha E_m\left(\frac{B}{0.3}\right)^{-\frac{3}{4}} \quad (11)$$

where k_v is the SRM, E_m is Young's modulus of the ground under the foundation bottom, B is the FW, B_r is the reference width of the loading plate used for the plate loading test to determine the SRM, and B_r = 0.3m in this study. α is a coefficient specified as 2 (for example) when E_m is evaluated using the N-values from the standard penetration tests to obtain the SRM values during an earthquake.

The variation of the N-value is large in relation to soil rigidity and no unified equation exists to express their

relationship. For example, in the JSHB, E_m is calculated as $2800N$. This study discusses the FW dependency of the SRM and not the method to calculate the Young's modulus of the ground using the N-value. Therefore, in the following, the SRM results obtained from the JSHB equations are shown as their changes by changing the FW under conditions where they are the same as the results of this study when B = 4m. Figure 8 compares the SRMs obtained in this study and the JSHB's. The SRM decreases by 50% from the JSHB equation if the FW is widened from 4m to 10m, however in this study, the SRM decreases by only 33%. Underestimation of the SRM in the case of foundation widening leads to overdesign. Therefore, the JSHB equation is not applicable for a wide foundation.

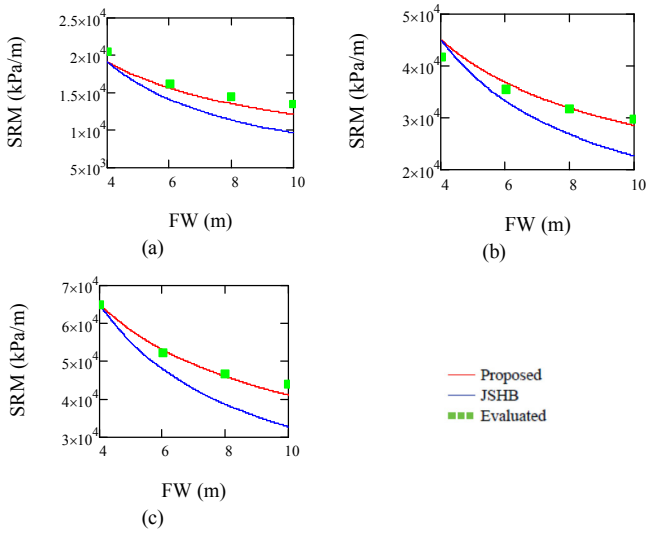

Fig. 8. FW dependency of SRM. (a) Case A, (b) Case B, (c) Case C.

D. Evaluation Method of RRM

The RRM is calculated using:

$$M = k_v I \theta \quad (12)$$

where M is the RRM, k_v is the SRM, I is the geometrical moment of inertia of the foundation bottom around the rotational center axis, and θ is the foundation's rotational angle.

Figure 7 shows that the SRM decreases as the load increases, so the change in the SRM must be considered according to the change in the rotational angle. The change in the rotational center position when increasing the load will also be considered. Figure 9 shows the change in the SR distribution when increasing the horizontal load for the condition B = 6m of Case B. The legend in the Figure is the value of the horizontal load. The SR is shown as an increment from that before horizontal loading. The position where the SR becomes zero should be regarded as the rotational center. The distance from the foundation edge to the rotational center is defined as the rotational radius, which decreases when the load increases. The value of the rotational radius was obtained by regression analysis when excluding the SR at the foundation edge. Figure 10 shows the relationship between the rotational angle and radius for the condition B = 6m of Case B. Here, the rotational radius is shown as a ratio to the FW. Figure 11 shows the relationship between the rotational angle and the SRM. Here, the SRM is shown as a ratio to its initial value. In the range where the rotational angle is minute, the rotational radius is half the FW, and the foundation rotates around its center. The rotational radius decreases as the rotational angle increases because the rear end of the foundation bottom floats. The higher the ground rigidity is, the more the rotational radius decreases. The SRM decreases with the increase in the rotational angle, as with the rotational radius. The decrease in the rotational radius and SRM when increasing the rotational angle results in the nonlinearity of the relationship between the RRM and the rotational angle (M-θ relationship).

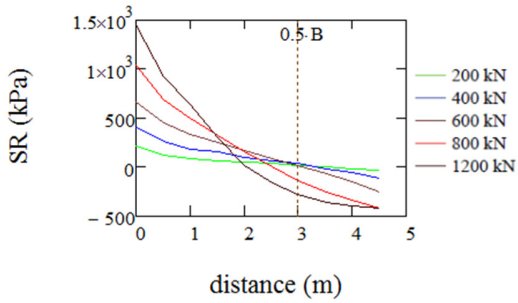

Fig. 9. Distribution of SR.

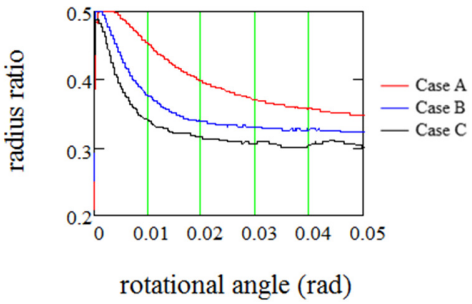

Fig. 10. Relationship between the rotational angle and the rotational radius.

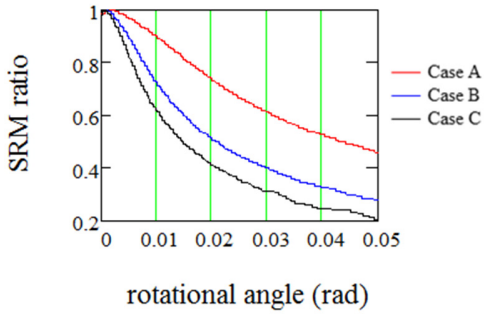

Fig. 11. Relationship between the rotational angle and the SRM.

Figure 12 shows the M-θ relationship for the condition B = 6m. The M-θ relationship shows a strong nonlinear characteristic because both the rotational radius and the SRM decrease with the increase in the rotational angle. The rotational angle where the RRM reaches the upper limit is

defined as the critical rotational angle. The higher the ground rigidity is, the smaller the critical rotational angle becomes. The critical rotational angles are 0.010rad, 0.005rad, and 0.003rad respectively for Cases A, B, and C. The critical rotational angles are similar for other FWs and do not depend on the FW but are strongly affected by the ground rigidity.

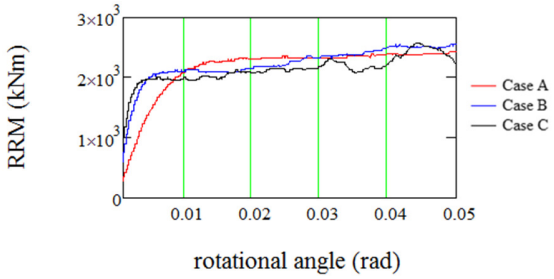

Fig. 12. M-θ relationship.

The reduction in shear rigidity of the ground significantly affects the nonlinearity of the SR. Figure 13 shows the relationship between the shear rigidity and the strain of the ground at the foundation bottom depth in each case. Here, the initial value (G_0 in (4)) normalizes the shear rigidity. The rotational angle of the foundation and the shear strain of the ground are equivalent in the range where the rotational angle is small. The shear strain corresponding to the critical rotational angle is evaluated. It corresponds to the shear strain where the shear rigidity is decreased to 15% of the initial value. Therefore, in this study, the shear strain when G/G_0 becomes 0.15 is the critical rotational angle. Furthermore, the reduction rates of the SRM and rotational radius corresponding to the critical rotational angle are both 0.9 and are independent of ground rigidity. The RRM is calculated using (13). The M-θ relationship is proposed as a simple bilinear characteristic considering the applicability to design practice.

$$\begin{aligned} M &= ak_v I\theta \quad (\theta \le \theta_c) \\ &= ak_v I\theta_c \quad (\theta > \theta_c) \end{aligned} \tag{13}$$

where θ_c is the critical rotational angle and a is a coefficient that considers the reduction in the SRM and rotational radius when the rotational angle reaches the critical value. Because the reduction in the rotational radius has a cubic effect on I, a is set to 0.9^4.

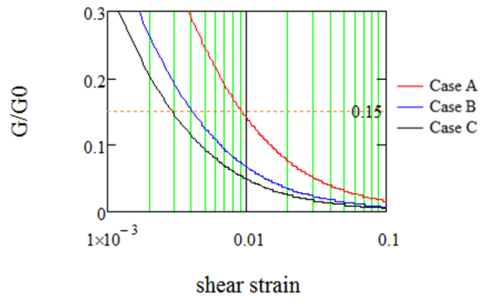

Fig. 13. Relationship between shear rigidity and shear strain.

Figures 14 and 15 compare the analytical values of the RRM under foundation widths of 6m and 8m respectively, with those values obtained by (13). The red line shows the analytical value and the blue line denotes the value according to (13). The proposed equation slightly underestimates the RRM for Case A. However, Case A's foundation is embedded in the soft soil layer of the N-value = 10, which is not frequently realized in design practice. For Cases B and C, the proposed equation evaluates well the RRMs.

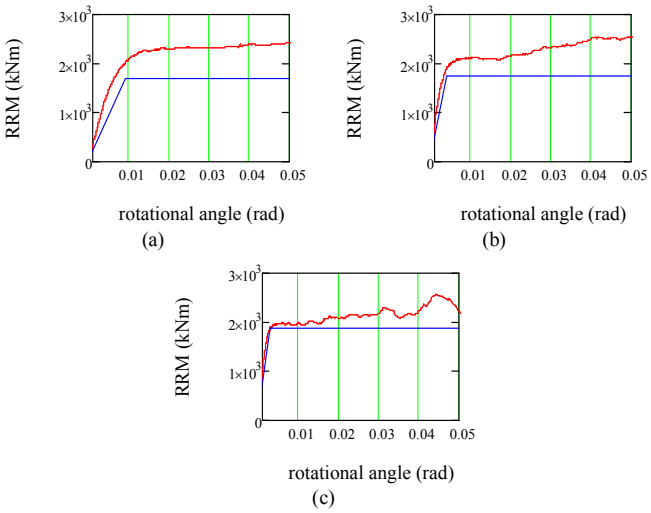

Fig. 14. M-θ Relationship (B = 6m). (a) Case A, (b) Case B, (c) Case C.

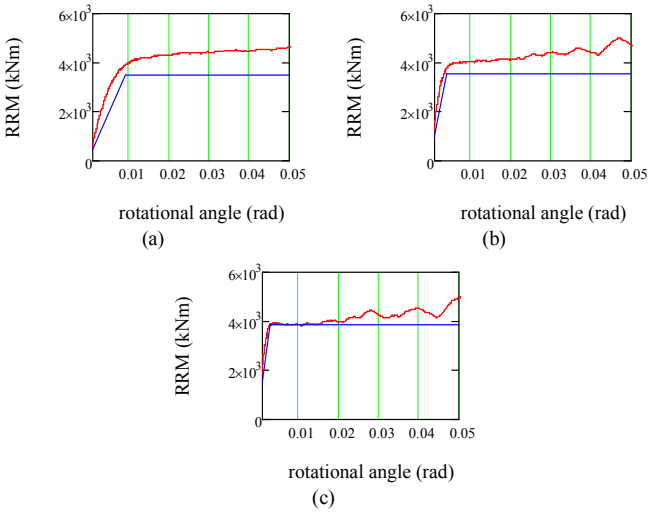

Fig. 15. M-θ relationship (B = 8m). (a) Case A, (b) Case B, (c) Case C.

IV. CONCLUSIONS

This study used the results of two-dimensional finite element analysis considering the nonlinearity of the ground and proposed the SRM and RRM calculation methods to be used for the seismic design of the embedded foundation. The main obtained conclusions are:

- Both compressive and shear strains occur in the ground when an inclined load is applied to the foundation. The compressive strain differs from position to position, however the shear strain does not differ significantly according to the position because it depends on the foundation's rotational angle. Therefore, the shear stress of the ground reaches the shear strength almost simultaneously when the rotational angle of the foundation becomes large and the shear strain increases sharply. Therefore, at positions other than the foundation edge, the SR does not reach the maximum value at the foundation edge, and the rotational angle of the foundation increases sharply. The design code overestimates the maximum SR value not only at the foundation edge, but also at other positions.
- A SRM calculation equation related to FW and ground rigidity was proposed. The SRM dependency on the FW was smaller than the assumption in the design code.
- When the horizontal load is large and the rotational angle increases, the SRM decreases under the influence of the nonlinearity of the ground, and the rotational radius decreases to half of the FW because the rear end of the foundation floats. Therefore, the M-θ relationship shows nonlinearity. This study proposed a calculation equation for evaluating the M-θ relationship using the reduction rate of the rotational radius and SRM when the rotational angle reaches the critical rotational angle, referring to the shear strain when the shear rigidity of the ground lowers to 0.15 of the initial value. The proposed equation is simple and bilinear considering its applicability to design practice and can evaluate RRM with high accuracy.

ACKNOWLEDGEMENTS

The analytical modeling for FEA was developed in collaboration with Daisuke Shibata. This research was supported by JSPS KAKENHI, Grant Number JP18K04324.

REFERENCES

[1] K. Terzaghi, "Evalution of Conefficients of Subgrade Reaction," *Géotechnique*, vol. 5, no. 4, pp. 297–326, Dec. 1955, https://doi.org/10.1680/geot.1955.5.4.297.

[2] R. Ziaie-Moayed and M. Janbaz, "Effective Parameters on Modulus of Subgrade Reaction in Clayey Soils," *Journal of Applied Sciences*, vol. 9, no. 22, pp. 4006–4012, 2009, https://doi.org/10.3923/jas.2009.4006.4012.

[3] J. Lee and S. Jeong, "Experimental Study of Estimating the Subgrade Reaction Modulus on Jointed Rock Foundations," *Rock Mechanics and Rock Engineering*, vol. 49, no. 6, pp. 2055–2064, Jun. 2016, https://doi.org/10.1007/s00603-015-0905-9.

[4] Nihon Dōro Kyōkai, *Specifications for highway bridges. Part 4*. Tokyo, Japan: Japan Road Association, 2002.

[5] T. Nagao and D. Shibata, "Experimental Study of the Lateral Spreading Pressure Acting on a Pile Foundation During Earthquakes," *Engineering, Technology & Applied Science Research*, vol. 9, no. 6, pp. 5021–5028, Dec. 2019, https://doi.org/10.48084/etasr.3217.

[6] T. Nagao, "An Experimental Study on the Way Bottom Widening of Pier Foundations Affects Seismic Resistance," *Engineering, Technology & Applied Science Research*, vol. 10, no. 3, pp. 5713–5718, Jun. 2020, https://doi.org/10.48084/etasr.3590.

[7] T. Nagao, "Effect of Foundation Width on Subgrade Reaction Modulus," *Engineering, Technology & Applied Science Research*, vol. 10, no. 5, pp. 6253–6258, Oct. 2020, https://doi.org/10.48084/etasr.3668.

[8] S. Iai, K. Ichii, H. Liu, and T. Morita, "Effective stress analysis of port structures," *Soils and Foundations*, no. Special, pp. 97–114, Sep. 1998.

[9] T. Nagao and P. Lu, "A simplified reliability estimation method for pile-supported wharf on the residual displacement by earthquake," *Soil Dynamics and Earthquake Engineering*, vol. 129, p. 105904, Feb. 2020, https://doi.org/10.1016/j.soildyn.2019.105904.

[10] T. Morita, S. Iai, H. Liu, K. Ichii, and Y. Sato, "Simplified Method to Determine Parameter of FLIP," PARI, Technical Note 0869, 1997.

[11] I. Suetomi and N. Yoshida, "Nonlinear Behavior of Surface Deposit during the 1995 Hyogoken-Nambu Earthquake," *Soils and Foundations*, vol. 38, pp. 11–22, Sep. 1998, https://doi.org/10.3208/sandf.38.Special_11.

[12] B. O. Hardin and V. P. Drnevich, "Shear Modulus and Damping in Soils: Design Equations and Curves," *Journal of the Soil Mechanics and Foundations Division*, vol. 98, no. 7, pp. 667–692, Jul. 1972, https://doi.org/10.1061/JSFEAQ.0001760.